J Therm Anal Calorim (2015) 122:437–447
DOI 10.1007/s10973-015-4928-y

Influence of ferrocene on smoke suppression properties and combustion behavior of intumescent flame-retardant epoxy composites

Lei Liu[1] · Xilei Chen[1] · Chuanmei Jiao[1]

Received: 3 November 2014 / Accepted: 11 February 2015 / Published online: 4 September 2015
© Akadémiai Kiadó, Budapest, Hungary 2015

Abstract This article mainly studies smoke suppression properties and synergistic flame-retardant effects of ferrocene ($Fe(C_5H_5)_2$) on intumescent flame-retardant epoxy resins (IFREP) using ammonium polyphosphate and pentaerythritol as intumescent flame retardants. The smoke suppression properties and flame retardancy of ferrocene on IFREP compositions were investigated by cone calorimeter test (CCT), scanning electron microscopy (SEM), thermogravimetric analysis-infrared spectrometry (TG-IR). Remarkably, CCT data revealed that the addition of ferrocene into IFREP compositions can significantly reduce heat release rate, total heat release, smoke production rate, and total smoke release. On the other hand, the SEM results showed that ferrocene can greatly improve the structure of char residue. The TG data indicated that ferrocene had different effects on the process of thermal degradation of the IFREP compositions. Moreover, the volatilized products formed on thermal degradation of IFREP compositions demonstrated that the volatilized products were H_2O, CO_2, CO, carboxylic acid, and aliphatic hydrocarbons according to the temperature of onset formation. Here, ferrocene is considered to be an effective smoke suppression agent and a good synergism with IFR in flame-retardant epoxy resins, which can greatly enhance the char residue.

Keywords Smoke suppression · Ferrocene · Flame retardant · Epoxy

✉ Chuanmei Jiao
jiaochm@qust.edu.cn

[1] College of Environment and Safety Engineering, Qingdao University of Science and Technology, Qingdao 266042, Shandong, People's Republic of China

Introduction

It is very well established now that the real killer in fires is, in most cases, the inhalation of smoke and toxic gases rather than thermal injury [1, 2]. The visibility impairing and narcotic irritating effect due to the evolution of smoke, toxic gases and irritant compounds can prevent a substantial number of fire victims from perceiving their possibilities of escape and hinder firemen trying to rescue them [3–7]. The smoke, smoke particulates, and some toxic compounds (chiefly carbon monoxide, CO and possibly other gases such as hydrogen cyanide, HCN) produced during the course of a real fire are known to cause morbidity and mortality in fire victims [8, 9]. In addition, the high temperature smoke containing a lot of heat can accelerate the spread of fire and lead to thermal damage [10]. As a result, reducing emissions of smoke and poisonous gases during a fire is very essential for preventing the loss of life.

Epoxy resin (EP) is a very important thermosetting material owing to its excellent mechanical and chemical properties. As a high performance material, EP is extensively used in many fields, such as adhesive, coating, laminating capsulation, electronic/electrical insulation, and composite applications [11–16]. Nevertheless, flammability is the major drawback of EP, restricting its potential applications. In addition, EP generates amounts of smoke and poisonous gas during combustion, causing damage to healthy people. Therefore, many strategies have been used to simultaneously inhibit flammability and the smoke release of polymeric materials during combustion [17–23]. In past decades, halogenated compounds which showed effective flame-retardant properties were commonly used as co-monomers or additive with epoxy resins to obtain fire-retardant materials. Unfortunately, research into the safety of flame retardants revealed some negative assessments of

halogen-containing flame retardants, such as the generation of corrosive, obscuring and toxic smoke [24–26]. In recent years, intumescent flame-retardant (IFR) additives have been widely utilized in the flame retardation of flammable polymers due to their excellent advantages of low toxicity, low smoke and low corrosion during combustion [27]. However, the sole utilization of IFR usually requires high content to achieve a good flame-retardant rating. A small amount of coadditives can significantly improve the thermal stability and flame-retardant properties, implying that they can enhance the efficiency of IFR. Various compounds have been used as coadditives, including iron compounds, lanthanum oxide, and fumed silica [28–31]. Thus, development of novel synergistic agents with IFR systems for high efficient flame-retardant EP can further explore the epoxy resins applications.

Recently, ferrocene has received considerable attention as an effective smoke suppressant and flame retardant [32, 33]. Extensive investigations have been carried out aiming at the effects of ferrocene on the flame retardancy and smoke suppression of polyvinyl chloride (PVC) [34–37]. Ferrocene is effective in the absence of halogen. And, the mechanism of smoke suppression has generally been attributed to the formation of iron (III) chloride, which acts as a Lewis acid and promotes char formation. In addition, char oxidation to oxides of carbon is also catalyzed [38, 39]. As far as we know, little work has been reported regarding the synergistic effects between ferrocene and IFR on the achievement of smoke suppression and flame-retardant properties in epoxy resins.

The purpose of the present work is to investigate the synergistic smoke suppression properties and flame-retardant effects between ferrocene and IFR in flame-retardant epoxy resins. The synergistic smoke suppression properties and flame-retardant effects were systematically investigated by cone calorimeter test (CCT), thermogravimetric analysis-infrared spectrometry (TG-IR). The scanning electron microscopy (SEM) analysis was used to further analyze how the structure of char determines smoke suppression properties of IFREP.

Experimental

Materials

Epoxy resin (bisphenol A epoxy acrylate resin), used as film-forming material was purchased from the Stanley Technology Co. Ltd., Shijiazhuang, China; methyltetrahydrophthalic anhydride (MTHPA; 98 % pure) curing agent was from Sitanlei Co. Ltd., Shijiazhuang, China; ammonium polyphosphate (APP) with particle size of 2500 mesh was purchased from new thin Metal and Chemical Co., Ltd., Guangzhou, China; pentaerythritol (PER) with particle size of 2500 mesh was purchased from new thin Metal and Chemical Co., Ltd., Guangzhou, China; IFR was obtained with the mass ratio of APP and PER is 3:1; ferrocene (particle size of 800 mesh) was purchased from the Zhicheng Trade Co., Ltd., Qingdao, China.

Preparation of samples

EP was mixed with ferrocene at room temperature using a high-speed disperser for 1.0 h to yield the blend. Then, IFR was added into the blend and stirred for 1.0 h. At last, MTHPA was added and stirred for 1.0 h. And the listing order is given in Table 1. The mixture was cured under 80 °C for 8.0 h, and 150 °C for 3.0 h to obtain flame-retardant epoxy composites.

Measurements

Cone calorimeter

The cone calorimeter (Stanton Redcroft, UK) tests were performed according to ISO 5660 standard procedures. Each specimen of dimensions 100 × 100 × 3 mm^3 was wrapped in aluminum foil and exposed horizontally to an external heat flux of 50 kW m^{-2}.

Scanning electron microscope (SEM)

Scanning electron microscope (SEM, JSM-6700F) was used to examine the structures of char residues after CCT. The samples were coated with a thin layer of gold by sputtering before the SEM imaging. An accelerating voltage of 5 kV was applied.

Thermogravimetric analysis/infrared spectrometry (TG-IR)

Thermogravimetric analysis/infrared spectrometry (TG-IR) of the sample was performed using a DT-50 (Setaram, France) instrument that was interfaced to a FTIR (TENSOR27, Bruker Co. Germany) spectrometer. About 10.0 mg of sample was put in an alumina crucible and heated from ambient temperature to 750 °C. The heating rates were set as 20 K min^{-1} (nitrogen atmosphere, flow rate of 20 mL min^{-1}).

Results and discussion

Cone calorimeter test

Heat release rate

Cone calorimeter test is one of the most effective bench-scale methods for comparing and evaluating the

Table 1 The formulations of flame-retardant epoxy composites

Sample code	Epoxy/mass%	MTHPA/mass%	IFR/mass%	Ferrocene/mass%
EP-0	55.6	44.4	–	–
EP-1	39.0	31.0	30.0	–
EP-2	39.0	31.0	29.5	0.5
EP-3	39.0	31.0	29.0	1.0
EP-4	39.0	31.0	28.0	2.0
EP-5	39.0	31.0	27.0	3.0

flammability characteristics of polymer materials and provides a wealth of information from its simulation of real world fire conditions. Heat release rate (HRR), especially peak heat release rate (PHRR) is one of the most important parameters for predictors of fire hazards, which in turn determines other parameters. The measured HRR curves of all flame-retardant epoxy samples at 50 kW m^{-2} are shown in Fig. 1 for comparison. It can be found from Fig. 1 that the ignition time of EP-0 is 70 s. And, EP-0 burns faster after ignition, and a sharp PHRR appears with a PHRR value of 914 kW m^{-2}. EP-0 has a single peak, implying that the sample gradually burns, whereas samples with IFR all have multi-peak phenomena. The first peak of HRR appears before the intumescent residual chars take place, and the insulating char layer formed on the surface of the samples can protect the composites from both the mass and the heat transfer; thus, the HRR values decrease. The peak HRR values take place again due to the fact that the increasing temperature destroys the partial charred material on the unexposed surface [40]. In the case of EP-1 with only IFR, the ignition time decrease from 70 to 65 s in comparison with that of EP-0. The first PHRR value of EP-1 is 149 kW m^{-2}, and the second PHRR value is 282 kW m^{-2} which is much lower than that of EP-0. This

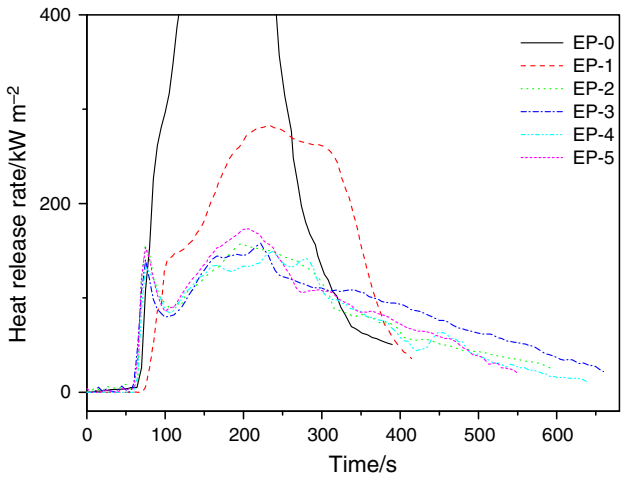

Fig. 1 Heat release rates of EP composites at a flux of 50 kW m^{-2}

can be explained by the fact that APP can release ammonia at the beginning of heating. Meanwhile, polyphosphoric acid formed by the elimination of ammonia from APP can react with hydroxyl bonds of PER to produce phosphoric ester, which thermally decomposes at higher temperatures with the formation of three-dimensional network structures. Furthermore, the C–H bonds for EP can be dehydrogenated and oxidized with formation of C–O–OH groups on the backbone. Incorporation of IFR results in a complicated network through cross-linking reactions between IFR and EP. This charred layer acting as a barrier prevents the heat transfer between the flame zone and the substrate, thus reduces the HRR and related parameters [41, 42]. In the case of the samples with both IFR and ferrocene, the addition of ferrocene further decreases the PHRR value as compared to that of EP-1. The first PHRR values are greatly reduced to 155, 140, 133, and 154 kW m^{-2}, respectively. And, the second PHRR values are 158, 157, 149, and 173 kW m^{-2}, respectively. When 2 mass% ferrocene was added to IFREP, the PHRR value for EP-4 decreases greatly and is the lowest among all the samples. It can be seen from Fig. 1 that the HRR curves of the cured epoxy samples with both IFR and ferrocene form a typical flat shape with a plateau between 100 and 550 s. The dramatically decrease in PHRR of the samples with the addition of ferrocene can be interpreted that ferrocene begins to decompose when the temperature reaches decomposition levels, and its decomposition can be described by a five-step reaction process. In this reaction zone, FeC_5H_5 can be formed by the ferrocene reduction reaction involving H and O, which eventually brings about the formation of the iron atom. Meanwhile, iron atom may enter into the catalytic cycle for H and OH recombination, which can consume radicals in the combustion chain reaction and suppresses explosion flame propagation [33]. During combustion progress, iron atom can also facilitate the release of ammonia from APP, and form Fe^{n+} because of multiple valency of Fe. And, APP can react with Fe^{n+} which takes as bridges, and the formation would increase the molecular weight and lead to a stabilization of the APP, which will increase the viscosity of the melt and the difficulty of extracting small molecules as volatiles during

burning and pyrolysis [43]. Moreover, ammonia and other volatilizes can make the mixture of the carbonaceous residue swell leading to the formation of the intumescent char residue. It should be pointed out that the ignition times of the samples from EP-2 to EP-5 shorten to 48, 44, 46, 45 s, respectively. The reason why the ignition time decreases is that the samples with different additives show different thermal response behaviors in the CCT, and they may expand before ignition in the CCT, leading to the distance between the surface of cone small and the sample. This means that the expansion process is not uniform. At the same time, the increasing radiation heat flux will accelerate EP decomposing, causing short ignition time [44]. The above results indicate that the addition of ferrocene can remarkably improve the flame-retardant properties of IFREP. The scheme of the combustion mechanism for IFREP system with ferrocene is shown in Scheme 1.

Mass loss

Figure 2 shows mass loss as a function of combustion time for EP composites. The mass loss behavior is related to the behavior of heat release and smoke suppression, and the decrease in mass loss maybe ascribe to the char residue and its morphological structure on the surface of the composites [45, 46]. It is observed that there is no residue left for EP-0 when the combustion process is completed, but the char yield of EP-1 is increased to 33 mass% at approximately 425 s. EP-1 shows significantly lower mass loss, which indicates that the addition of IFR can catalyze the formation of a protective rigid layer to prevent both the mass and the heat transfer. However, this layer is not compact enough and breaks quickly, bringing about large mass loss later. It should be pointed out that the average mass loss rate of the samples from EP-1 to EP-5 is larger than that of EP-0 between 40 and 90 s. This phenomenon is attributed to the low decomposition temperature of APP, and this early decomposition of the IFR system is advantageous in increasing the fire-proofing properties of the material [47, 48]. In addition, the mass loss rate of the samples with both IFR and ferrocene is much lower than that of EP-0 after approximately 80 s. At the end of burning, the char residue mass of the samples from EP-2 to EP-5 is 46, 42, 47, and 44 mass%, which are much higher than that of EP-1. When the loading of ferrocene increases to 2 mass%, EP-4 shows the highest char residue among all flame-retardant samples. This fact indicates that ferrocene can catalyze ammonia and polyphosphoric acid elimination, cross-linking, and decomposition reactions between EP and IFR, and plays an important role in the hindered diffusion of volatile decomposition products due to the barrier effect of the compact char residue. And, this

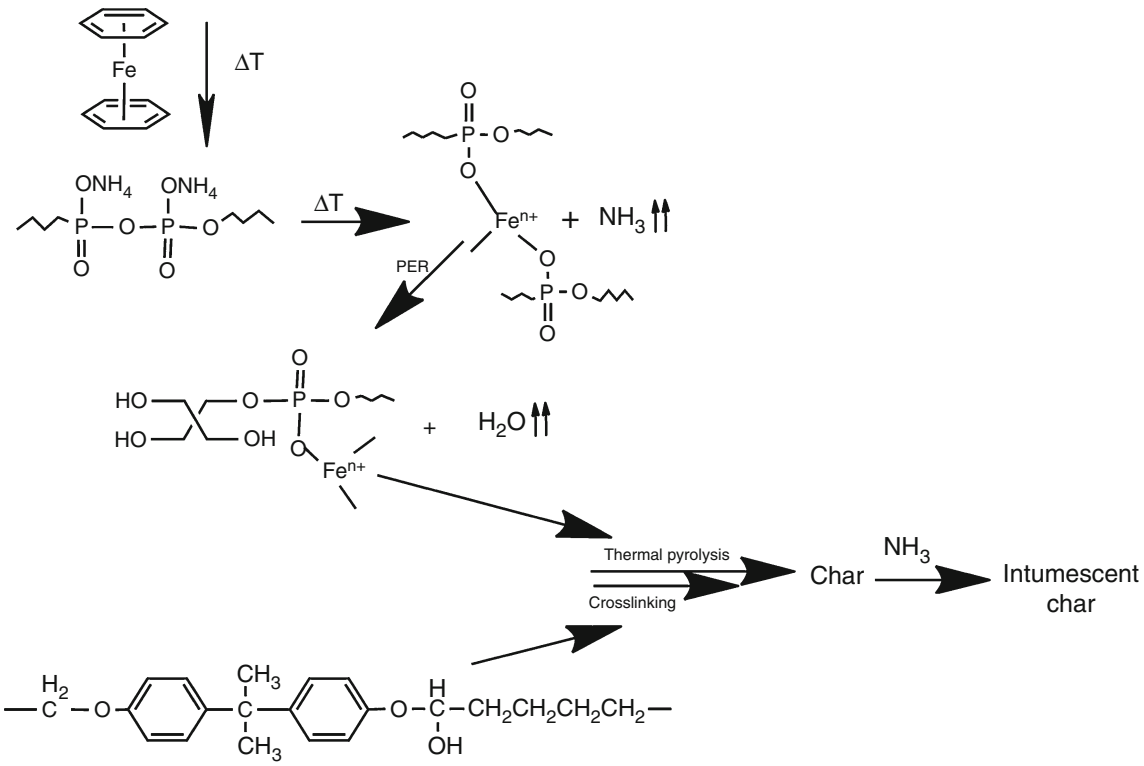

Scheme 1 Possible reaction mechanisms of char formation during the combustion of IFREP system with ferrocene

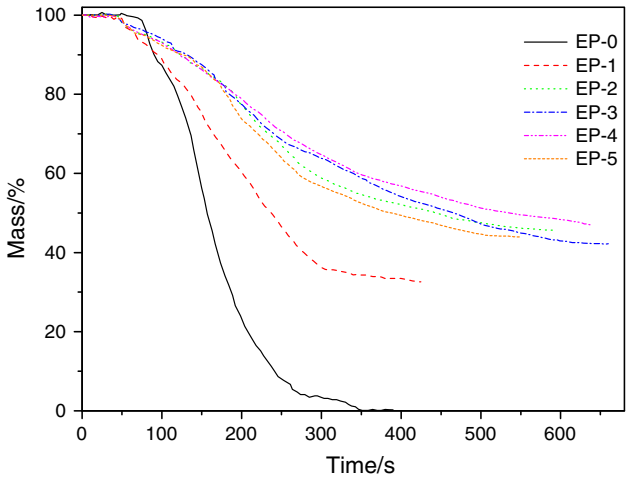

Fig. 2 Mass loss curves of EP composites at a flux of 50 kW m^{-2}

compact char residue formed on the surface of the sample can effectively improve its fire safety. It can be concluded that the improved flammability properties of these samples are mainly due to difference in condensed-phase decomposition processes and not to a gas-phase effect.

Total heat release

Figure 3 displays the curves of total heat release (THR) for EP samples. THR is another important parameter for the flame-retarded materials, which correlates well with carbonaceous charring, flame inhibition-mainly reducing combustion efficiency in the flame, and fuel dilution-including the replacement of polymer in the condensed phase [36]. In particular, the gradient of THR curve can be assumed as representative of fire spread [49]. From Fig. 3, EP-0 has released a total heat of 124.2 mJ m^{-2}, while EP-1 just releases 64.2 mJ m^{-2}, indicating flame spread speed slows down. In the case of the samples containing both IFR and ferrocene, the flame spread speed further decreases. It suggests that during the burning process ferrocene could serve to generate beneficial intumescent char layers on the surface of the matrix, which acts as a thermal insulation layer to inhibit polymer pyrolysis and prevent the evolution of combustible gases to feed the flame and also separate oxygen from burning materials. When 2 mass% ferrocene is added to IFREP system, the THR value for EP-4 decreases from 64.2 to 46.2 mJ m^{-2}, indicating its char layer structure is compact enough to restrict flame spread.

Total smoke release

The total smoke release (TSR) values of EP composites are illustrated in Fig. 4. It can be found that when IFR is used, the TSR values of the samples from EP-1 to EP-5 are higher than that of EP-0 at the beginning of heating, due to the low decomposition temperature of APP. And, the distinction between EP-0 and the flame-retardant samples is apparent after 150 s. The TSR values of all samples are 3928, 2412, 671, 843, 743, and 660 m^2 m^{-2}, respectively. Clearly, the incorporation of ferrocene could significantly decrease the TSR values at the end of burning. There are two basic smoke suppression mechanisms of ferrocene in burning composites. First, ferrocene can increase the viscosity of the melt and the stability of the char layer by acting with APP during the process of pyrolysis and combustion. This stable char residue can act as a protective barrier, and effectively restrict the transfer of mass and heat between gas and condensed phases [42]. Secondly, Fe^{n+} ions provided by ferrocene behave as an ideal radical scavenger and consequently can be used to restrain the attack of the free radicals [50]. And, they are especially effective in chemically removing certain volatile fuels which are responsible for promoting the burning of the specimens and the formation of smoke particulates [51].

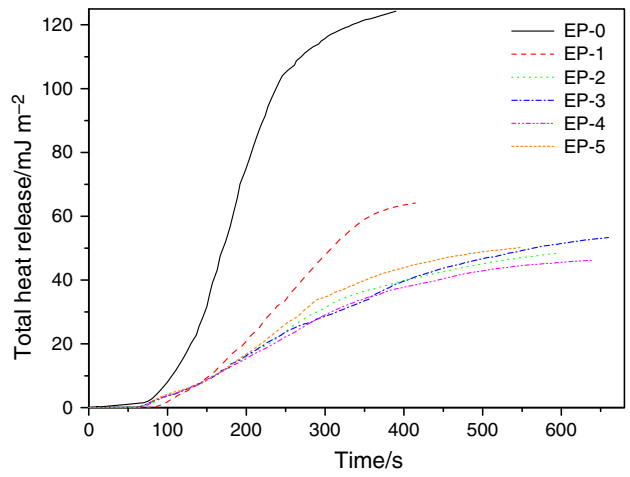

Fig. 3 Total heat release of EP composites at a flux of 50 kW m^{-2}

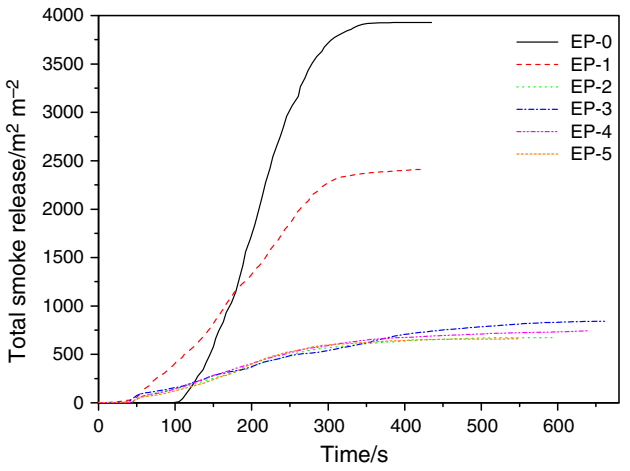

Fig. 4 Total smoke release of EP composites at a flux of 50 kW m^{-2}

Smoke production rate

Smoke in a real fire means more risk of suffocation, and thus smoke performance of flame-retardant material is regarded as an important parameter used to evaluate fire hazard. The smoke production rate (SPR) curves of EP composites are presented in Fig. 5. The peak SPR value of EP-0 is 0.294 m^2 s^{-1} at 170 s, whereas the peak SPR value of EP-1 is 0.103 m^2 s^{-1} at 152 s, indicating the addition of IFR can decrease the SPR of the composite. And, the time to peak SPR of EP-1 is much shorter than that of EP-0. This is the reason that at the initial stage of heating, the increasing surface temperature would bring about rapid decomposition of APP and formation of smoke particles on the surface of EP-1. It is clear that ferrocene can slow the SPR, and hence, the peak SPR values of samples containing both IFR and ferrocene decrease from 0.103 m^2 s^{-1} of EP-1 to 0.063, 0.075, 0.057, and 0.047 m^2 s^{-1}, respectively. It is found that the curves of the samples with IFR and ferrocene have the homologous phenomenon with the HRR curves in the CCT. Moreover, it should be pointed out that the time to the peak SPR value of samples from EP-2 to EP-5 are 50, 47, 50, and 51 s, respectively. The significant decrease in peak SPR value by ferrocene can be explained as follows: ferrocene can promote charring and enhance the quality of char, and the protective char layer on the surface can not only give a less disturbing low volatilization rate, but also hinder oxygen and heat from spreading into the non-combusted substrate [44].

Smoke factor

Figure 6 gives the smoke factor (SF) as a function of time for EP composites, which is the product of PHRR and TSR [52]. SF is recognized to be a more accurate measure of the rate at which smoke is released. At the end of burning, the SF value of EP-0 is up to 3669 mW m^{-2}, while that of EP-1 is dramatically reduced to 681 mW m^{-2}. It is very clearly that the addition of IFR can significantly reduce the SF values of IFREP composites. The SF values of the samples with both IFR and ferrocene are 84, 133, 114, 135 mW m^{-2}, respectively. The addition of ferrocene further decreases the smoke generation with respect to EP-1, which is in accordance with the above results of SPR and TSR. It proves the good smoke suppression properties of ferrocene.

Photographs and scanning electron microscopy of char residue

Figure 7 presents the digital photographs and SEM images obtained for the exterior char residues of EP samples after CCT. The formation of efficient carbon layer can insulate the heat transfer and prevent the diffusion of the oxygen and the volatile products efficiently. The photographs demonstrate that EP-0 was burnt out, whereas more dense and coherent chars were formed with the addition of IFR. The char residue of EP-1 presents a porous surface, and the samples containing both IFR and ferrocene present compact and continual char residues. It should be pointed out that the surface of the char residue becomes tighter and denser than any other residue by increasing the loading of ferrocene up to 2 mass%, which is in consistent with lowest HRR, THR, and a series of data tested by cone calorimeter. This phenomenon may be due to the fact that the catalyst in an appropriate addition range can exert good catalytic effect in a certain system, whereas exceeding the amount of catalyst may show no improvements or even worsen the catalytic effect.

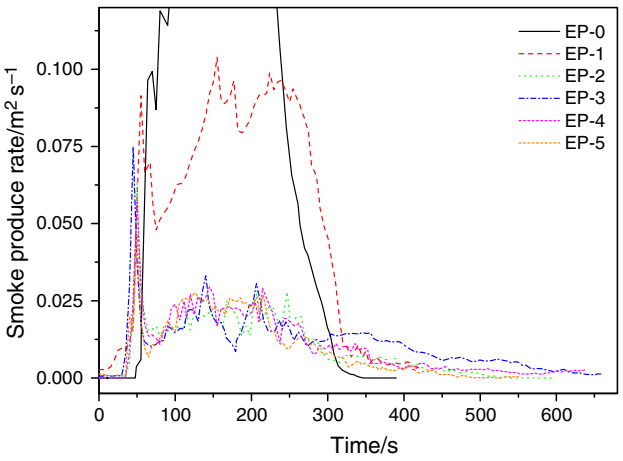

Fig. 5 Smoke production rates of EP composites at a flux of 50 kW m^{-2}

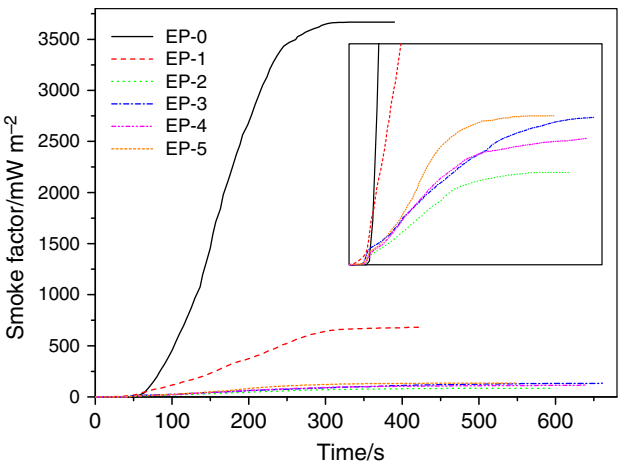

Fig. 6 Smoke factors of EP composites at a flux of 50 kW m^{-2}

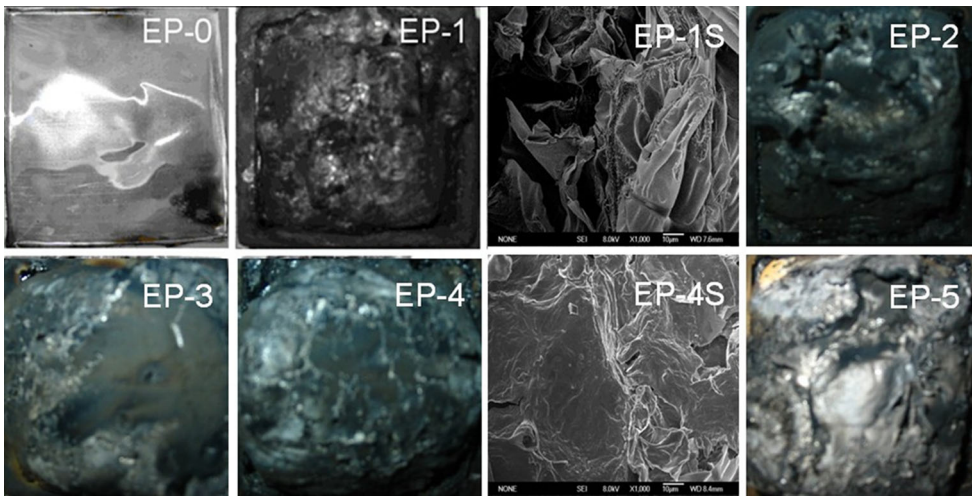

Fig. 7 Digital photographs and SEM of char residue from EP composites

In order to elucidate the structure of the char formed during combustion and further explore how the formation of residual char affects the combustion of the flame-retarded epoxy composites, the microstructures of the char after combustion were characterized by SEM. Figure 7 illustrates SEM images obtained for the exterior char residues of EP-1 and EP-4 magnified 1000×, respectively. As for EP-1, the carbon layer presents an irregular appearance including some holes and many leakage bubbles, due to the low strength of the char structure and low viscosity of the melted coating. Additionally, the air in these large holes can lower heat transference, but air convection will increase the speed of heat transference at the same time [53]. The surface of the char residue from EP-4 emerges a more compact and continual lamellar structure compared with EP-1, because the addition of ferrocene can contribute to form the structure of cross-linked carbonaceous residue which restrains the heat release and smoke generation.

Fire performance index (FPI) and fire growth index (FGI)

The FPI and FGI calculated from the directly measured data of cone calorimeter experiments are usually regarded as the overall assessment of the fire safety of a material. FPI (m^2 s kW^{-1}) and FGI (kW m^{-2} s^{-1}) are defined as the ratio of the time to ignition (TTI) to the PHRR value and the ratio of the PHRR value to the time to PHRR (TTP), respectively [44]. Therefore, the higher the value of the FPI or the lower the value of the FGI, the higher is the material's safety rank [54, 55]. The FPI and FGI values of EP samples are revealed in Fig. 8. It can be seen that the FPI increases and the FGI decreases with the incorporation of ferrocene compared to that of EP-1. That is, there is more compact char residue formed on the surface of the sample with ferrocene. The compact char residue can restrain combustible gases, so the released flammable gases can be complete combusted, which improves the fire safety of IFREP composites. For the samples containing ferrocene and IFR, EP-4 owns the lowest FGI value and highest FPI value, demonstrating that it gets the highest safety rank among all samples.

Thermogravimetric analysis (TG)

A thermogravimetric analyzer (TG) is one of the most widely used techniques for evaluating the thermal stability of various polymers. The thermal stability of flame-retardant material has a great relationship with the release of decomposition products and the formation of char layer on the surface of samples [56]. The relevant data show the temperatures at which 5.0 % degradation occurs, $T_{0.05}$, as a measure of the onset of the degradation. TG and derivative thermogravimetric (DTG) curves are shown in Fig. 9a, b, respectively. As can be seen from Fig. 9, the onset decomposition temperature of EP-0 is about 390.5 °C, and the maximum mass loss temperature is 422.8 °C. The mass loss rate of EP-0 notably slows down after 500 °C, and the residual char is 11.5 % at 700.0 °C. The initial decomposition temperature of EP-1 is 325.4 °C, which is lower than EP-0. The noticeable decrease in the decomposition temperature is responsible for the low decomposition temperature of APP, which can reduce the formation temperature of carbon layer, and thus prevent EP composites from further thermal degradation [44]. In addition, EP-1 sample left about 28.6 mass% at 700 °C, which is much higher than that of EP-0 (11.5 mass%). As usual, thermal degradation of EP has one step which is related to the chain scissions of EP and the destruction of the C–C and C–O bonds on the main chain. However, there are two main

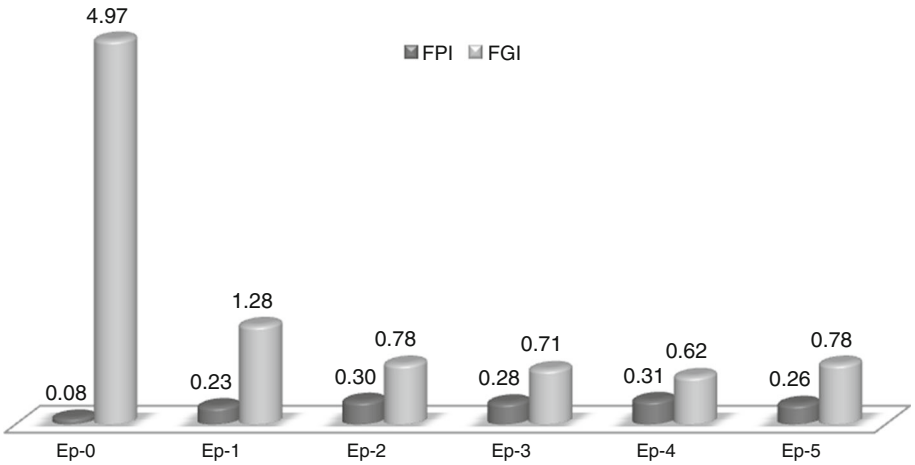

Fig. 8 FPI and FGI of EP composites at a flux of 50 kW m^{-2}

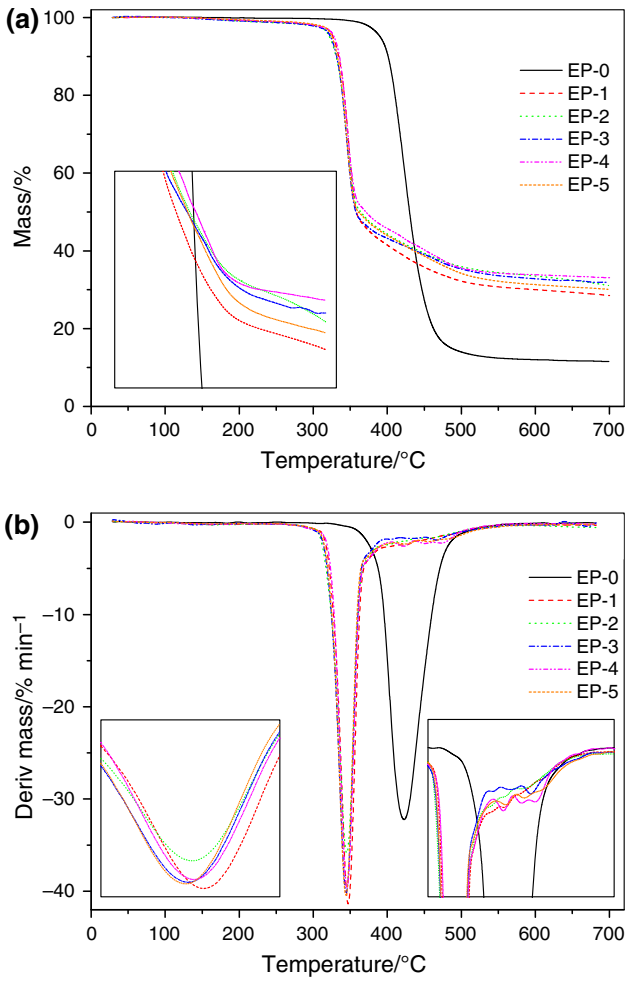

Fig. 9 TG and DTG curves of EP composites

decomposition stages of EP-1 in the temperature ranges of 300–400 and 400–500 °C, with two corresponding differential thermogravimetric (DTG) peaks. And, these two thermal degradation steps are attributed to ammonia and polyphosphoric acid release, and decomposition of the polyphosphoric acid chain, respectively.

It can be seen from Fig. 9a, b that ferrocene may react with IFR to form a more thermally stable structure with more char residue left, while the catalytic activity on the polymer is not very obvious from TG data under N_2. In the case of the samples from EP-2 to EP-5, their initial decomposition temperatures are 322.1, 323.6, 328.4, and 324.1 °C, respectively, which are lower than that of EP-1. Moreover, ferrocene further increases the mass of flame-retardant EP composites at high temperature. The residues of the samples with ferrocene are about 31.1, 31.9, 33.1 and 30.1 mass% at 700 °C, respectively. When the loading of ferrocene increases to 2 mass%, EP-4 owns the highest thermal property among all samples. That is to say, the presence of ferrocene in IFREP tends to promote the formation of a charred residue which is more stable than that of EP-1, and it contributes to effective smoke suppression and flame retardancy. The radical trapping by the Fe^{n+} can also enhance thermal stability of EP [57]. Thermal degradation of the sample with ferrocene has two decomposition stages: the first decomposition stage is responsible for the reaction between APP and ferrocene, whereas the second stage is mainly caused by the rupture of the EP main chains and the destruction of the C–C and C–O bonds on the main chain.

TG-IR characterization of EP-0/EP-1/EP-4 composites

TG-IR technique can directly analyze the volatilized products, which provides insight into the thermal degradation mechanisms [56]. The characteristic TG-IR spectra of pyrolysis products of the EP samples at different times during the decomposition process are presented in Fig. 10. Peaks in the regions of around 3230–3550, 2800–3150, 2250–2400, 1700–1850, 1250–1500, and 950–1150 cm^{-1}

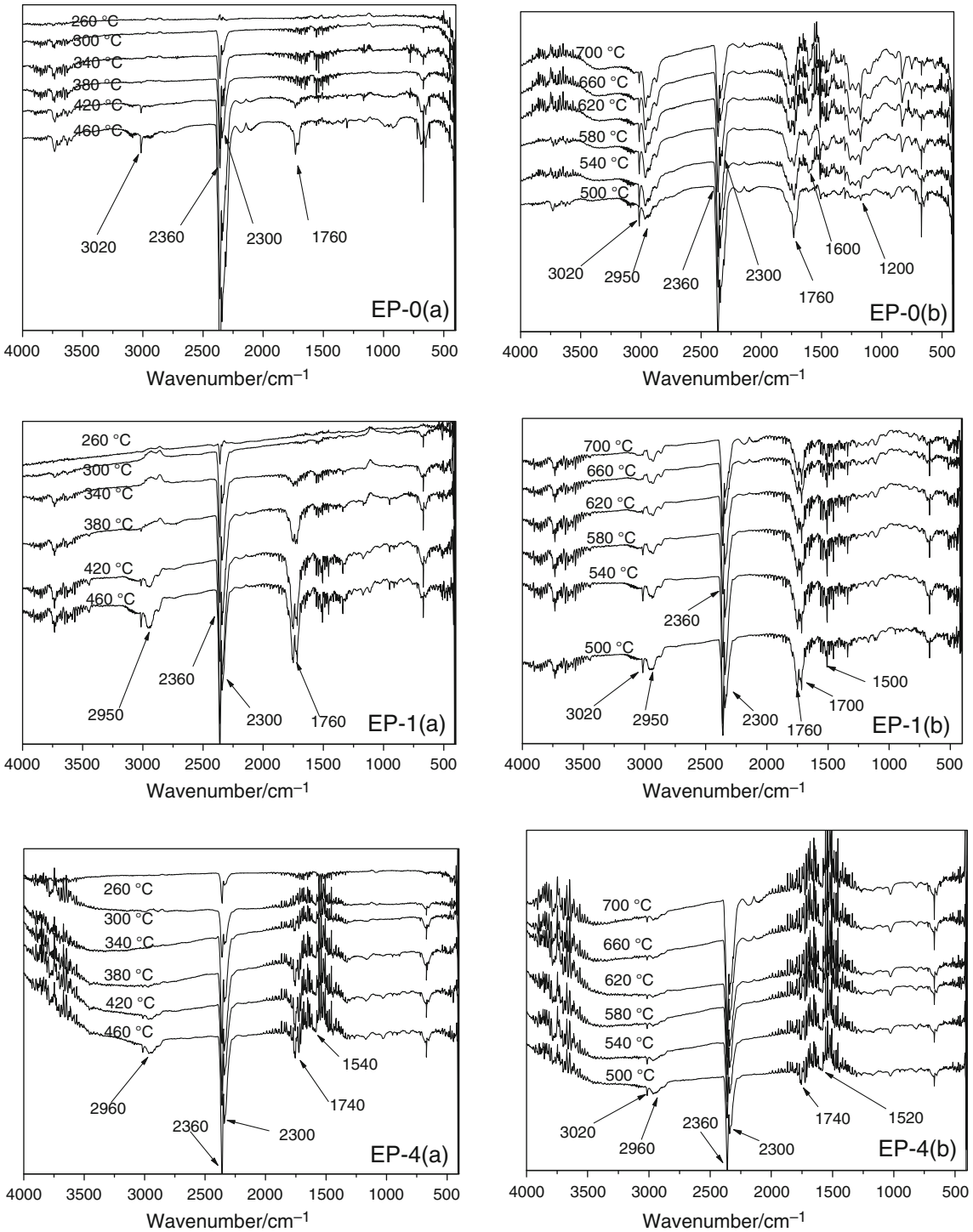

Fig. 10 TG-IR spectra of volatilized products from EP-0 (**a**, **b**), EP-1 (**a**, **b**), and EP-4 (**a**, **b**) at various temperature

are highly noted. Some of the volatilized decomposition products of the EP are unambiguously identified by characteristic strong FTIR signals, such as H_2O (3230–3550 cm^{-1}), CO_2 (2300–2400 cm^{-1}), CO (2250–2300 cm^{-1}), carboxylic acid (1700–1850 cm^{-1}), and aliphatic hydrocarbons (2800–3150, 1250–1500, and 950–1150 cm^{-1}). In the process of depolymerization, the main products of the thermal decomposition of EP are compounds containing H_2O, CO_2, CO, carboxylic acid, and aliphatic hydrocarbons. The depolymerization processes of these three samples are significantly different according to Fig. 10. In the case of EP-0, it decomposes drastically with

lots of pyrolysis products, whereas the decomposition rate of EP-1 is slowed down. In particular, the decomposition rate of EP-4 is slowed down further when ferrocene is introduced into the EP composites.

As shown in Fig. 10, the decomposition of these three composites do not happen below 260 °C because there is almost no infrared signal under this temperature. The main decomposition products will be detected with the temperature increasing to 300 °C. As for EP-0, the peak appears at 2360 cm^{-1} indicating the appearance of CO_2. And, the intensity of characteristic peaks for CO_2 reaches a maximum with the temperature increasing to 460 °C (460 °C for EP-1, 580 °C for EP-4). Moreover, a maximum signal at 2950 cm^{-1} attributed to aliphatic hydrocarbons can be detected at 500 °C (500 °C for EP-1, 460 °C for EP-4). The formation of CO, CO_2 and aliphatic hydrocarbons are detected, probably due to the rupture of the EP main chains and the destruction of the C–C and C–O bonds on the main chain. In fact, the further decomposition of carbonic anhydride structures can also bring about the elimination of volatilized CO and CO_2 by the formations of alkane and aromatic compounds [56]. The maximum signal intensity appears at 1760 cm^{-1} due to the acid anhydride being observed with the temperature increasing to 500 °C (540 °C for EP-1, 500 °C for EP-4). This is mainly caused by that acid anhydride can be formed at high temperature in result of the reaction among carboxylic acid molecules. In addition, there are some aromatic compounds (characteristic peaks at 1505 cm^{-1}) formed in the degradation of EP-1 and EP-4. At the end of decomposition, the signal intensity of the pyrolysis products declined gradually, which reflects the decomposition rate of the mixture is slowed down.

Conclusions

As to all the results of IFREP containing ferrocene (IFREP/ferrocene) tested by CCT, SEM, and TG-IR, we can draw the following conclusions. First, ferrocene can help to change the structure of char residue layer that restrain the heat release and smoke generation. Second, ferrocene represents dramatically excellent smoke suppression properties in flame-retardant epoxy composites based on IFR. Third, the synergistic flame-retardant effect and smoke suppression between ferrocene and IFR is very apparent. In summary, the synergistic smoke suppression and flame-retardant properties between ferrocene and IFR in epoxy composites are excellent. Combining ferrocene and IFR as a system has the wide application prospect in smoke suppression fields.

Acknowledgements The authors gratefully acknowledge the National Natural Science Foundation of China (Nos. 51106078; 51206084) and the out-standing Young Scientist Research Award Fund from Shandong Province (BS2011CL018).

References

1. Yan YW, Chen L, Jian RK. Intumescence: an effect way to flame retardance and smoke suppression for polystryene. Polym Degrad Stab. 2012;97(8):1423–31.
2. Dong Y, Gui Z, Hu Y. The influence of titanate nanotube on the improved thermal properties and the smoke suppression in poly (methyl methacrylate). J Hazard Mater. 2012;209:34–9.
3. Purser DA. Toxic product yields and hazard assessment for fully enclosed design fires. Polym Int. 2000;49(10):1232–55.
4. Cassuto J, Tarnow P. The discotheque fire in Gothenburg 1998: a tragedy among teenagers. Burns. 2003;29(5):405–16.
5. Beyer G. Flame retardant properties of EVA-nanocomposites and improvements by combination of nanofillers with aluminium trihydrate. Fire Mater. 2001;25(5):193–7.
6. Martinka J, Kačíková D, Hroncová E, Ladomerský J. Experimental determination of the effect of temperature and oxygen concentration on the production of birch wood main fire emissions. J Therm Anal Calorim. 2012;110(1):193–8.
7. Ye L, Zhang Y, Wang S, Gao G, Liu J, Zhou Y, Liu H. Synergistic effects and mechanism of $ZnCl_2$ on intumescent flame-retardant polypropylene. J Therm Anal Calorim. 2014;115(2):1065–71.
8. Irvine DJ, McCluskey JA, Robinson IM. Fire hazards and some common polymers. Polym Degrad Stab. 2000;6(3):383–96.
9. Omaye ST. Metabolic modulation of carbon monoxide toxicity. Toxicology. 2002;180(2):139–50.
10. Zhou R, Zhang W, Zhao D. Computational simulation of smoke temperature diffusion in high-rise buildings fires. Res J Appl Sci Eng Technol. 2013;5(6):2078–83.
11. Kinjo N, Ogata M, Nishi K, Kaneda A. Epoxy molding compounds as encapsulation materials for microelectronic devices. Adv Polym Sci. 1989; 88:1–48.
12. Chen H, Jacobs O, Wu W. Effect of dispersion method on tribological properties of carbon nanotube reinforced epoxy resin composites. Polym Test. 2007;26(3):351–60.
13. Guo Y, Bao C, Song L. In situ polymerization of graphene, graphite oxide, and functionalized graphite oxide into epoxy resin and comparison study of on the flame behavior. Ind Eng Chem Res. 2011;50(13):7772–83.
14. Wu K, Song L, Hu Y. Synthesis and characterization of a functional polyhedral oligomeric silsesquioxane and its flame retardancy in epoxy resin. Prog Org Coat. 2009;65(4):490–7.
15. Guo Q, Huang Y, Zhang YY, Zhu LR, Zhang BL. Curing behavior of epoxy resins with a series of novel curing agents containing 4,4′-biphenyl and varying methylene units. J Therm Anal Calorim. 2010;102(3):915–22.
16. Jiao CM, Zhuo JL, Chen XL, Li SX, Wang H. Flame retardant epoxy resin based on bisphenol A epoxy resin modified by phosphoric acid. J Therm Anal Calorim. 2013;114(1):253–9.
17. Wang X, Hu Y, Song L. Thermal degradation mechanism of flame retarded epoxy resins with a DOPO-substitued organophosphorus oligomer by TG-FTIR and DP-MS. J Anal Appl Pyrol. 2011;92(1):164–70.
18. Bao C, Guo Y, Song L. In situ preparation of functionalized graphene oxide/epoxy nanocomposites with effective reinforcements. J Mater Chem. 2011;21(35):13290–8.
19. Azeez AA, Rhee KY, Park SJ. Epoxy clay nanocomposites—processing, properties and applications: a review. Compos Part B Eng. 2013;45(1):308–20.
20. Wan J, Li C, Bu ZY. A comparative study of epoxy resin cured with a linear diamine and a branched polyamine. Chem Eng J. 2012;188:160–72.
21. Cheng XE, Shi W. Synthesis and thermal properties of silicon-containing epoxy resin used for UV-curable flame-retardant coatings. J Therm Anal Calorim. 2011;103(1):303–10.

22. Gao M, Wu W, Yan Y. Thermal degradation and flame retardancy of epoxy resins containing intumescent flame retardant. J Therm Anal Calorim. 2009;95(2):605–8.
23. Agrawal S, Narula AK. Curing and thermal behaviour of a flame retardant cycloaliphatic epoxy resin based on phosphorus containing poly (amide–imide) s. J Therm Anal Calorim. 2014;115(2):1693–703.
24. Mauerer O. New reactive, halogen-free flame retardant system for epoxy resins. Polym Degrad Stab. 2005;88(1):70–3.
25. Lin HT, Lin CH, Hu YM. An approach to develop high-T_g epoxy resins for halogen-free copper clad laminates. Polymer. 2009;50(24):5685–92.
26. Rybiński P, Janowska G, Dobrzyńska R, et al. Effect of halogenless flame retardants on the thermal properties, flammability, and fire hazard of cross-linked EVM/NBR rubber blends. J Therm Anal Calorim. 2014;115(1):771–82.
27. Wang X, Song L, Yang H, et al. Synergistic effect of graphene on antidripping and fire resistance of intumescent flame retardant poly (butylene succinate) composites. Ind Eng Chem Res. 2011;50(9):5376–83.
28. Chen XL, Liu L, Jiao CM, et al. Influence of ferrite yellow on combustion and smoke suppression properties in intumescent flame-retardant epoxy composites. High Perform Polym. 2014;. doi:10.1177/0954008314553644.
29. Chen XL, Liu L, Zhuo JL, et al. Influence of iron oxide green on smoke suppression properties and combustion behavior of intumescent flame retardant epoxy composites. J Therm Anal Calorim. 2014;. doi:10.1007/s10973-014-4193-5.
30. Chen XL, Liu L, Zhuo JL, et al. Influence of organic-modified iron–montmorillonite on smoke-suppression properties and combustion behavior of intumescent flame-retardant epoxy composites. High Perform Polym. 2014. doi:10.1177/0954008314544341.
31. Wang L, Yang W, Wang B, et al. The impact of metal oxides on the combustion behavior of ethylene-vinyl acetate coploymers containing an intumenscent flame retardant. Ind Eng Chem Res. 2012;51(23):7884–90.
32. Carty P, Metcalfe E, Saben TJ. Thermal analysis of plasticised PVC containing flame retardant/smoke suppressant inorganic and organometallic iron compounds. Fire Saf J. 1991;17(1):45–56.
33. Yu MG, Zheng K, Zheng LG, et al. Experimental study on gas explosion suppression based on ferrocene. J Coal Sci Eng. 2013;19(3):358–62.
34. Gallo E, Schartel B, Braunb U, Russoa P, Aciernoa D. Fire retardant synergisms between nanometric Fe_2O_3 and aluminum phosphinate in poly(butylene terephthalate). Polym Adv Technol. 2011;22:2382–91.
35. Zhang B, Yan XY, Shibata K. Thermogravimetric-mass spectrometric analysis of the reactions between oxide (ZnO, Fe_2O_3 or $ZnFe_2O_4$) and polyvinyl chloride under inert atmosphere. Mater Trans. 2000;41:1342–50.
36. Laoutid F, Ferry L, Lopez-Cuesta JM, Crespy A. Flame-retardant action of red phosphorus/magnesium oxide and red phosphorus/iron oxide compositions in recycled PET. Fire Mater. 2006;30:343–58.
37. Kashiwagi T, Grulke E, Hilding J, Harris R, Awad W, Douglas J. Thermal degradation and flammability properties of poly(propylene)/carbon nanotube composites. Macromol Rapid Commun. 2002;23:761–5.
38. Gholamian F, Shabanian M, Shahrokh M. Magnetic and thermal properties of novel poly (ether-amide)/Fe_3O_4 nanocomposite containing phosphine oxide group. J Clust Sci. 2013;24(1):177–88.
39. Liu ZL, Wang HB, Lu QH, et al. Synthesis and characterization of ultrafine well-dispersed magnetic nanoparticles. J Magn Magn Mater. 2004;283(2):258–62.
40. Liu Y, Zhao J, Deng CL, et al. Flame-retardant effect of sepiolite on an intumescent flame-retardant polypropylene system. Ind Eng Chem Res. 2011;50(4):2047–54.
41. Kandola BK, Horrocks AR. Complex char formation in flame-retarded fibre-intumescent combinations—II. Thermal analytical studies. Polym Degrad Stab. 1996;54(2):289–303.
42. Tang Y, Hu Y, Song L, Zong RW, Gui Z, Fan WC. Preparation and combustion properties polypropylene-polyamide-6 of flame retarded alloys. Polym Degrad Stab. 2006;91(2):234–41.
43. Zhang P, Hu Y, Song L, Lu HD, Wang J, Liu QQ. Synergistic effect of iron and intumescent flame retardant on shape-stabilized phase change material. Thermochim Acta. 2009;487:74–9.
44. Chen XL, Jiang YF, Jiao CM. Smoke suppression properties of ferrite yellow on flame retardant thermoplastic polyurethane based on ammonium polyphosphate. J Hazard Mater. 2014;266:114–21.
45. Lin M, Li B, Li Q, et al. Synergistic effect of metal oxides on the flame retardancy and thermal degradation of novel intumescent flame-retardant thermoplastic polyurethanes. J Appl Polym Sci. 2011;121(4):1951–60.
46. Schartel B, Hull TR. Development of fire-retarded materials-interpretation of cone calorimeter data. Fire Mater. 2007;31:327–54.
47. Cai YB, Li Q, Wei QF, Wu YB, Song L, Hu Y. Structures, thermal stability, and crystalline properties of polyamide6/organic-modified Fe-montmorillonite composite nanofibers by electrospinning. J Mater Sci. 2008;43(18):6132–8.
48. Ullah S, Ahmad F, Megat-Yusoff PSM. Effect of boric acid with kaolin clay on intumescent fire retardant coating. J Appl Sci. 2011;11(21):3645–9.
49. Chiang CL, Ma CCM. Synthesis, characterization and thermal properties of novel epoxy containing silicon and phosphorus nanocomposites by sol–gel method. Eur Polym J. 2002;38:2219–24.
50. Marinović-Cincović M, Popović MČ, Novaković MM, Nedeljković JM. The influence of β-FeOOH nanorods on the thermal stability of poly (methyl methacrylate). Polym Degrad Stab. 2007;92(1):70–4.
51. Carty P, White S, Price D, Lu L. Smoke-suppression in plasticised chlorinated poly (vinyl chloride) (CPVC). Polym Degrad Stab. 1999;63(3):465–8.
52. Ricciardi MR, Antonucci V, Zarrelli M, Giordano M. Fire behavior and smoke emission of phosphate-based inorganic fire-retarded polyester resin. Fire Mater. 2012;36:203–15.
53. Chen XL, Jiao CM, Li SX, Sun J. Flame retardant epoxy resins from bisphenol-A epoxy cured with hyperbranched polyphosphate ester. J Polym Res. 2011;18:2229–37.
54. Fang SL, Hu Y, Song L, Zhan J, He QL. Mechanical properties, fire performance and thermal stability of magnesium hydroxide sulfate hydrate whiskers flame retardant silicone rubber. J Mater Sci. 2008;43:1057–62.
55. Jiao CM, Chen XL, Zhang J. Synergistic effects of Fe_2O_3 with layered double hydroxides in EVA/LDH composites. J Fire Sci. 2009;27:465–79.
56. Chen XL, Jiao CM. Thermal degradation characteristics of a novel flame retardant coating using TG-IR technique. Polym Degrad Stab. 2008;93:2222–5.
57. Kong Q, Lu H, Chen Z, et al. Synthesis and properties of polystyrene/Fe-montmorillonite nanocomposites using synthetic Fe-montmorillonite by bulk polymerization. J Mater Sci. 2005;40(17):4505–9.